

# LONGITUDINAL BEAM TRANSPORT IN THE ALICE IR-FEL FACILITY

F. Jackson<sup>#</sup>, D. Angal-Kalinin, J. K. Jones, P. H. Williams, STFC Daresbury Laboratory,  
ASTeC & Cockcroft Institute, UK

A. Wolski, University of Liverpool and Cockcroft Institute, UK

## Abstract

The ALICE facility at Daresbury Laboratory is an energy recovery test accelerator which includes an infra-red oscillator-type free electron laser (IR-FEL). The longitudinal transport functions (including  $R_{56}$  and  $T_{566}$ ) in the ALICE accelerator lattice are studied in this paper by use of precision time-of-arrival methods. The results allow characterisation of the triple bend achromat (TBA) arcs and compression chicane of the lattice. The relevance of the results to the operational performance of ALICE as an IR-FEL facility and a THz source is discussed.

## INTRODUCTION

The ALICE (Accelerators and Lasers in Combined Experiments) facility at Daresbury laboratory (see Fig. 1) is described elsewhere [1]. An IR-FEL has operated since 2010, and the facility has also been used as a THz source. Both these applications rely on short compressed bunches (bunch length of  $\sim$  ps) and an important aspect of the machine is the longitudinal transport.

The design for the energy recovery loop was isochronous arc followed by a 4-dipole compressor of  $R_{56} = 0.28$  m, followed by an arc with  $R_{56} = -0.28$  m [2]. Although the THz and FEL sources have operated for some years, the detailed quantitative verification of the longitudinal transport has not been performed. The compressed bunch profile has been measured, but the behaviour of the lattice in practice has not been fully understood. The most obvious example of this is in the use of the sextupoles in the first arc (ARC1), which usually have not been used according to the design for THz and FEL machine set-ups (in practice usually only the first of the two sextupoles has been observed to optimise/improve the THz or FEL output).

In order to improve the quantitative understanding of the longitudinal transport, a programme of bunch time-of-flight measurements was pursued, using the various BPMs located around the ALICE beam transport system. These studies build on measurements already performed in [3][4].

## MEASUREMENT METHOD

Measurement of the transport matrix elements  $R_{56}$  and  $T_{566}$  require bunch path length to be measured as a function of the beam energy. This was achieved by measuring the time-of-arrival (TOA) of bunches at a BPM by the raw bunch BPM signal on a high resolution oscilloscope (100 ps sampling resolution or better). The time-of-arrival of the bunch is then taken as, for example, the time-at-zero-crossing or 50%-max of the BPM signal,

and this enables a mean time of arrival measurement (taken over many macropulses) with accuracy of less than 1 ps. This mean time-of-arrival is then converted into relative path length simply by multiplying by  $c$ . The path length is measured while varying the beam energy and the resulting data can be fitted with a polynomial to extract  $R_{56}$ ,  $T_{566}$  [4]. It becomes apparent during analysis that the effective  $R_{56}$  and  $T_{566}$  experienced by the beam may depend on beam energy, which is important because the real beam energy is not a well-defined and constant reference energy; like any other machine parameter it may drift and vary (by the order of  $\sim$  1%) in pragmatic optimisation of the machine.

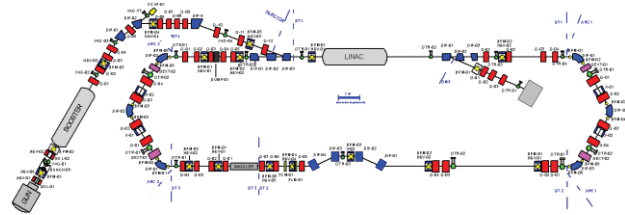


Figure 1: Layout of the ALICE accelerator.

## POST LINAC LONGITUDINAL TRANSPORT

### First Arc Transport, No Sextupole Correction

The energy dependent path length in the post-linac lattice was measured via the method described above at both the exit of the first arc (ARC1) and the exit of the compression chicane, using BPMs located there. This was repeated for several different strengths of the outer quadrupoles in the first arc (AR1-Q1/Q4), which are the main knobs for tuning the  $R_{56}$  in the compression stage of the beam transport [5].

The  $R_{56}$  values for each quadrupole setting were extracted by defining the reference momentum and fitting parabolas to the path length vs  $\Delta p/p$  curves, the linear coefficient yielding  $R_{56}$  (the quadratic coefficient yield  $T_{566}$ ). This is shown in Fig. 2. One can clearly visualise the relative sizes of  $R_{56}$ ,  $T_{566}$  by how pronounced the parabola appears, thus the measurements post-chicane (relatively large  $R_{56}$ ) appear much more 'linear' than those post arc. It can be clearly seen from the extracted  $R_{56}$  values (lower plot Fig. 2) that the transport through the arc becomes isochronous at a certain quadrupole strength, and at this condition the total  $R_{56}$  at the chicane exit is around -32 cm (the design value is -28cm). It can also be inferred that the chicane contributes a more-or-less constant contribution to the total post-linac  $R_{56}$  as the arc quadrupoles are varied, as expected.

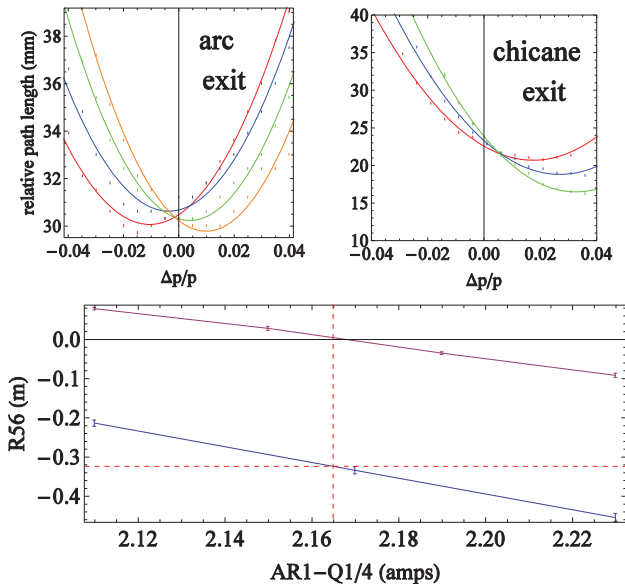


Figure 2: Post-linac longitudinal transport. Upper plots show the path length vs beam energy at the arc exit (left) and chicane exit (right); the colours indicate different arc quadrupole strengths. The lower plot shows the  $R_{56}$  at the arc exit (magenta) and chicane exit (blue) vs the arc quadrupole strength.

### ARC1 Isochronous and Zero Dispersion Condition

In the ideal ALICE lattice the first arc should be both isochronous and dispersion free at the exit. This condition relies on setting the arc quadrupole strengths to a unique set of values.

The dispersion and  $R_{56}$  at the arc exit was measured as a function of the outer quadrupoles to test if this condition was fulfilled. Using the BPM at the arc exit the beam position and TOA/path length were measured as a function of the beam energy to obtain  $R_{16}$ ,  $R_{56}$  by fitting parabola as described above. The results are shown in Fig. 3, where in addition, the theoretical values of  $R_{16}$  and  $R_{56}$  calculated using the ELEGANT [6] software package.

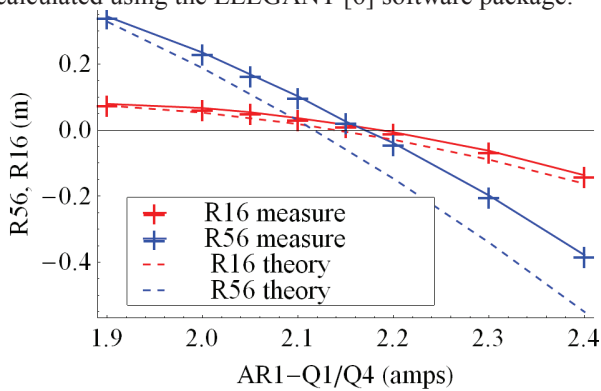


Figure 3: Dispersion ( $R_{16}$ ) and  $R_{56}$  of the first arc measured (solid lines) and predicted using ELEGANT (dashed lines).

It can be seen from Fig. 3. that the first arc approximately reaches the condition of isochronicity and

zero dispersion as the outer quadrupole strength is varied between 2.1 and 2.2 amps (the inner quadrupoles were set to approximately the design value). There is also a reasonable agreement between theory and measurement.

### Sextupole Influence on Longitudinal Transport and Alignment

The effect of the first arc sextupoles on  $T_{566}$  has previously been observed [4]. It is also apparent that the sextupoles influence the arc  $R_{56}$  for beams not perfectly aligned with the sextupole. These features can be used to align the beam to the arc sextupoles using TOA measurements. For example, using the first dipole in the arc to steer the beam, the path length vs. energy curve can be plotted for different beam positions in the first sextupole (with the sextupole at max strength), as is shown in Fig. 4. From this data the sextupole-induced change in  $R_{56}$  for a given beam energy and dipole steering can be calculated which is shown in Fig. 5.

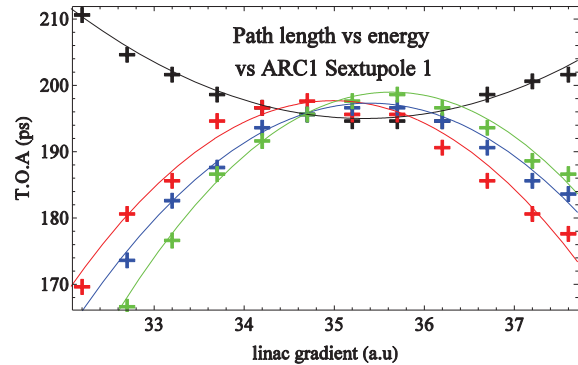


Figure 4: ARC1 TOA vs. energy for sextupole 1 off (black line) and sextupole on at maximum strength with different steering (coloured lines) of the first ARC1 dipole. The effect on the ARC1  $R_{56}$  and sextupole alignment can be deduced (see figure below).

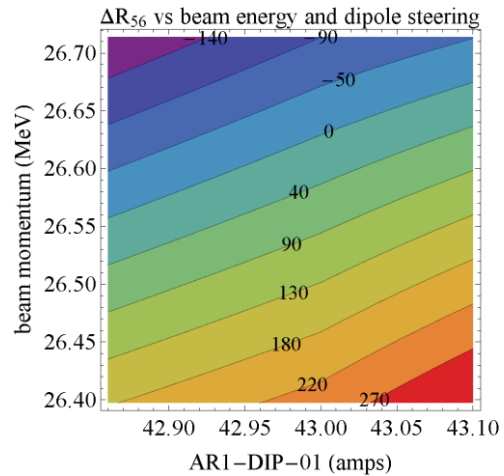


Figure 5: Sextupole induced change in  $R_{56}$  vs. beam momentum and steering through the dipole (the steering is done by varying the dipole AR1-DIP-01, immediately upstream of the sextupole). The labelled contours are the values of change in  $R_{56}$  (in mm) due to turning sextupole 1 from zero to full strength.

From Fig. 5, the zero contour gives the values of beam energy and dipole steering that centre the beam through the sextupole. These can be compared to the energy and dipole values that steer the beam to the reference trajectory i.e. bend the beam by exactly  $60^\circ$  (these can be estimated using the dipole current-to-field calibration and setting the beam energy using a screen downstream of the dipole). This comparison leads to an estimate of the offset of the sextupole with respect to the estimated reference orbit. This was estimated at around 2.5 mm for the first sextupole.

This procedure can then be repeated for the second sextupole in the first arc using the second arc dipole to steer the beam, and the sextupole offset again was estimated at around 2.5 mm compared to the estimated reference trajectory.

Thus neither sextupole are perfectly aligned with the estimated reference orbit. The absolute values of the estimates of the offsets are affected by accuracy in dipole calibration, and alignment of the screen by which the energy is measured. In real situations the beam may not be set to the reference trajectory and thus the effect of the sextupoles on  $R_{56}$  may be larger or smaller than these offsets imply. ALICE historically has not used detailed beam-based alignment procedures, thus the use of the sextupoles in ALICE set-ups probably significantly affects  $R_{56}$  and thus linear bunch compression, not merely the  $T_{566}$  RF curvature correction.

## INJECTOR LONGITUDINAL TRANSPORT

It has been observed during experience with the operation of the IR-FEL, and from the THz signal, that injector magnet settings have a strong effect. While FEL lasing to a given level can be established with different injector settings, small changes in injector quadrupole strengths can significantly enhance or suppress the IR-FEL radiation. The dynamics of the injector is non-trivial, with space charge and ballistic and magnetic bunching effects all potentially important [3].

To gain a more quantitative understanding of the magnetic bunching TOA measurements were carried out in the injector to measure the longitudinal transport elements. A BPM at the entrance to the main linac and the injector beam energy was varied in analogy to the post-linac method described above. In preliminary measurements, two injector quadrupoles were adjusted by small amounts (15% of their nominal setting) and the resulting extracted  $R_{56}$  varied by several cm. These results are illustrated in Fig. 6. The observation of this sensitivity of  $R_{56}$  to injector quadrupoles is supported by ELEGANT calculations. There may also be effects due to  $R_{51}$ ,  $R_{52}$  in Fig. 6 that have not been identified and quantified in detail. The sensitivity of the IR-FEL and THz to injector magnet settings could thus be partly explained by the sensitivity of the longitudinal transport in the injector.

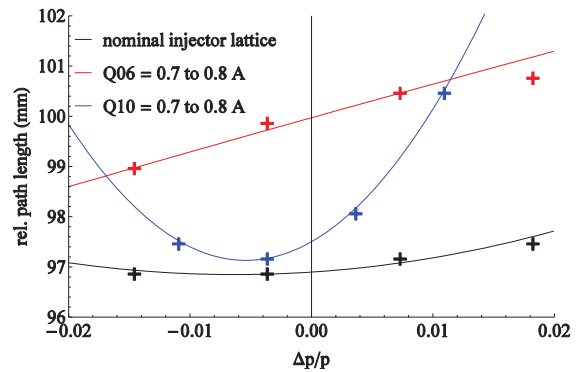


Figure 6: Measured path length vs beam energy in the injection line for nominal (black) set-up and set-ups where quadrupole strengths are changed by  $\sim 15\%$  (red and blue). The lines are best fit curves to the measured data points.

## CONCLUSIONS AND PRACTICAL IMPLICATIONS

The measurements of the longitudinal transport functions post-linac confirm the design behaviour of the TBA arcs and compression chicane, the key feature of which is the constant  $R_{56}$  of the chicane and the flexibility of  $R_{56}$  in the arc using the outer quadrupoles.

These measurements also indicate the sensitivity of the longitudinal transport functions  $R_{56}$ ,  $T_{566}$  to the beam energy, an important feature since the beam energy is often ‘tweaked’ during operation when developing practical machine set-ups for THz production or IR-FEL optimisation. The effective  $R_{56}$ ,  $T_{566}$ , and thus the compression, experienced by the bunch depends on the local shape of the path length vs. energy curve at the specific energy of the bunch. It may also be inferred that if there are bunch-to-bunch energy variations in the train the final compressed bunch length will also vary bunch-to-bunch.

Finally the quantitative estimation of sextupole alignment presented here may be useful in future in ensuring correct sextupole alignment and more efficient  $T_{566}$  RF curvature correction.

## REFERENCES

- [1] Y. Saveliev et al, “ALICE: Status, Developments and Scientific Programme”. IPAC ‘12, Albuquerque.
- [2] G. Gerth et al, “Start-to-end Simulations of the Energy Recovery Linac Prototype FEL”, FEL ‘04, Trieste.
- [3] F. Jackson, “Longitudinal Beam Dynamics at the ALICE Accelerator R&D Facility”, IPAC ‘12, Albuquerque.
- [4] F. Jackson, “Electron Beam Dynamics in the ALICE IR-FEL Facility”, FEL ‘12, Nara.
- [5] H. Owen and B. Muratori, “Choice of Arc Design for the ERL Prototype at Daresbury Laboratory”, EPAC ‘05, Lucerne.
- [6] M. Borland, Advanced Photon Source LS-287, September 2000.